Meshless methods for conservation laws

D. Hietel[1], M. Junk[2], J. Kuhnert[1], and S. Tiwari[1]

[1] Fraunhofer-Institut für Techno-und Wirtschaftsmathematik,
Gottlieb-Daimler-Straße, Geb. 49, 67663 Kaiserslautern, Germany

[2] Fachbereich Mathematik, Universität Kaiserslautern,
Erwin-Schrödinger-Straße, 67663 Kaiserslautern, Germany

Summary. In this article, two meshfree methods for the numerical solution of conservation laws are considered. The Finite Volume Particle Method (FVPM) generalizes the Finite Volume approach and the Finite Pointset Method (FPM) is a Finite Difference scheme which can work on unstructured and moving point clouds. Details of the derivation and numerical examples are presented for the case of incompressible, viscous, two-phase flow. In the case of FVPM, our main focus lies on the derivation of stability estimates.

1 Introduction

Meshfree techniques play an increasing role as solution methods for conservation laws. Practically, all meshfree methods are based on clouds of points, where each point carries the relevant information for the problem to be solved. One of the biggest advantages of these methods is that no mesh has to be established. Generating a grid can be very costly, sometimes it is even the dominating part in the problem. Compared to that, it is relatively simple to establish a point cloud, even within very complex geometries. Moreover, the cloud is easy to maintain or to adapt locally. Due to the free movement of the points, an optimal adaptivity of the cloud is provided towards changes in the geometry or towards movement of free surfaces as well as phase boundaries.

Among the pioneering meshfree methods, Smoothed Particle Hydrodynamics (SPH) is certainly the most famous [10]. SPH is a Lagrangian idea, which is based on the movement of finite mass points. However, for a long time, SPH was suffering from several problems, among them stability and consistency. Facing these problems, the development of meshfree methods went into various directions, starting in the early nineties. On one hand, people tried to improve SPH. One idea was to avoid inconsistency problems of SPH by reproducing kernel methods [30], another idea was to improve the approximation properties of SPH by the introduction of so called Moving Least Squares (MLS) ideas [5, 15]. On the other hand, many new types of meshfree methods were developed. Widely used methods are the Element Free Galerkin (EFG) idea [23] or the Partition of Unity Method (PUM) [8]. As the EFG and PUM ideas provide the possibility to carry out Finite Element computations on gridfree structures, the present paper introduces meshfree Finite Volume (FV) and Finite Difference (FD) concepts.

In section 2, we present the Finite Volume Particle Method (FVPM), which incorporates FV ideas into a meshfree framework [7]. In particular, the approach uses the concept of numerical flux functions and guarantees conservation on a discrete level. As we show in section 2, the similarity to classical Finite Volume schemes allows us to derive stability results using standard arguments. For numerical results obtained with FVPM, we refer to [7, 12, 24, 31].

In section 3, we concentrate on the Finite Pointset Method (FPM) which is a general Finite Difference Method for conservation laws on a meshfree basis [15, 16]. The latest FPM development which covers the discretization of the incompressible Navier-Stokes equations with multiple phases is presented.

2 The Finite Volume Particle Method

2.1 Derivation

The Finite Volume Particle Method (FVPM) has been developed in an attempt to combine features of SPH (Smoothed Particle Hydrodynamics) with Finite Volume Methods (FVM) [7]. To explain the idea, we consider the problem to find a function $u : [0,T] \times \mathbb{R}^d \to \mathbb{R}$ which satisfies

$$\frac{\partial u}{\partial t} + \mathrm{div}_{\boldsymbol{x}} \boldsymbol{F}(u) = 0, \qquad u(0,\boldsymbol{x}) = u^0(\boldsymbol{x}). \tag{1}$$

In the classical Finite Volume Method, conservation laws like (1) are discretized by introducing a Finite Volume mesh on $\mathbb{R}^d$ and integrating (1) over each volume element (see, for example, [6, 14]). To reformulate this procedure on a more abstract level, we note that a mesh gives rise to a particular *partition of unity* which is generated by the indicator functions of the elements. More specifically, if $\mathbb{R}^d$ is the disjoint union of mesh cells $C_i \subset \mathbb{R}^d$, then the functions $\chi_i = \mathbf{1}_{C_i}$ have the property $\chi_i \geq 0$, and $\sum_i \chi_i = 1$ where the sum is locally finite because at every $\boldsymbol{x} \in \mathbb{R}^d$, at most one function χ_i is nonzero (the one for which $\boldsymbol{x} \in C_i$). The Finite Volume scheme is then obtained by taking χ_i as test functions in a weak formulation of (1). In this context, the basic idea in FVPM is to choose a *smooth* partition of unity instead of a mesh-based partition. Let us therefore assume that a smooth, locally finite partition of unity $\{\psi_i\}_{i\in I}$ is given on $\mathbb{R}^d$, i.e. smooth and compactly supported functions $\psi_i : \mathbb{R}^d \to \mathbb{R}$ with $\psi_i \geq 0$ and $\sum_i \psi_i = 1$ where $\psi_i(\boldsymbol{x}) \neq 0$ for only finitely many indices at every $\boldsymbol{x} \in \mathbb{R}^d$ (the functions ψ_i are called *particles*). Such a partition can be constructed using a shape function W which is smooth, compactly supported around the origin, and strictly positive on its support, for example, a radially symmetric cubic spline, or the d-fold tensor product of a one-dimensional compactly supported function (in the first case, $\operatorname{supp} W$ is a d-dimensional ball, and in the second case, the support is an axis parallel cube). Then given a suitable set of points $\boldsymbol{x}_i \in \mathbb{R}^d$, $i \in I$ and some $h > 0$, we define scaled and shifted versions of W whose supports cover $\mathbb{R}^d$

$$W_i(\boldsymbol{x}) = W\left(\frac{\boldsymbol{x} - \boldsymbol{x}_i}{h}\right), \qquad \bigcup_i \operatorname{supp} W_i = \mathbb{R}^d. \tag{2}$$

Finally, using Shephard's method [22], the partition of unity is built

$$\psi_i(\boldsymbol{x}) = \frac{W_i(\boldsymbol{x})}{\sigma(\boldsymbol{x})}, \qquad \sigma(\boldsymbol{x}) = \sum_k W_k(\boldsymbol{x}), \qquad \boldsymbol{x} \in \mathbb{R}^d \tag{3}$$

and the partition functions ψ_i are used as test functions for equation (1). Multiplying (1) with ψ_i and integrating over $\mathbb{R}^d$, we obtain after integration by parts

$$\frac{d}{dt}\int_{\mathbb{R}^d} \psi_i u \, d\boldsymbol{x} - \int_{\mathbb{R}^d} \boldsymbol{F}(u) \cdot \nabla\psi_i \, d\boldsymbol{x} = 0. \tag{4}$$

In order to split the flux integral into pairwise flux contributions between particle i and its neighboring particles j, we use the fact that $\sum_j \psi_j = 1$ and $\nabla(\sum_j \psi_j) = 0$ which leads to

$$\frac{d}{dt}\int_{\mathbb{R}^d} \psi_i u \, d\boldsymbol{x} - \sum_j \int_{\mathbb{R}^d} \boldsymbol{F}(u) \cdot (\psi_j \nabla\psi_i - \psi_i \nabla\psi_j) \, d\boldsymbol{x} = 0. \tag{5}$$

The first integral is obviously related to a local average of u

$$u_i^n = \frac{1}{V_i}\int_{\mathbb{R}^d} \psi_i u \, d\boldsymbol{x}|_{t=t_n}, \qquad V_i = \int_{\mathbb{R}^d} \psi_i \, d\boldsymbol{x}. \tag{6}$$

To approximate the second integral in (5), we note that, if u varies only slightly around $\bar{u}$ on the intersection of the supports of ψ_i and ψ_j, we have

$$-\sum_j \int_{\mathbb{R}^d} \boldsymbol{F}(u) \cdot (\psi_j \nabla\psi_i - \psi_i \nabla\psi_j) \, d\boldsymbol{x} \approx \boldsymbol{F}(\bar{u}) \cdot \boldsymbol{\beta}_{ij},$$

where

$$\boldsymbol{\beta}_{ij} = \int_{\mathbb{R}^d} \psi_i \nabla\psi_j - \psi_j \nabla\psi_i \, d\boldsymbol{x}. \tag{7}$$

Following the usual procedure in the Finite Volume discretization we approximate the flux

$$\boldsymbol{F}(\bar{u}) \cdot \boldsymbol{\beta}_{ij} = |\boldsymbol{\beta}_{ij}| \boldsymbol{F}(\bar{u}) \cdot \boldsymbol{n}_{ij}, \qquad \boldsymbol{n}_{ij} = \frac{\boldsymbol{\beta}_{ij}}{|\boldsymbol{\beta}_{ij}|} \text{ if } |\boldsymbol{\beta}_{ij}| \neq 0$$

in terms of the discrete values with the help of a numerical flux function

$$\boldsymbol{F}(\bar{u}) \cdot \boldsymbol{n}_{ij} \approx g(u_i, u_j, \boldsymbol{n}_{ij}).$$

Finally, using an explicit Euler discretization of the time derivative, we obtain a fully discrete approximation of (5)

$$u_i^{n+1} V_i = u_i^n V_i - \Delta t \sum_j |\boldsymbol{\beta}_{ij}| g(u_i^n, u_j^n, \boldsymbol{n}_{ij}), \qquad u_i^0 = \frac{1}{V_i} \int_{\mathbb{R}^d} \psi_i u^0 \, d\boldsymbol{x}. \tag{8}$$

Observe that (8) has exactly the structure of the classical Finite Volume Method [6, 14]. The only difference appears in the definition of the *geometric parameters* V_i and $\boldsymbol{\beta}_{ij}$. While they are integral expressions involving the partition of unity functions ψ_i in the case of FVPM, they are mesh related quantities in the classical Finite Volume case: V_i is the volume of cell C_i and $\boldsymbol{\beta}_{ij} = |\Gamma_{ij}| \boldsymbol{n}_{ij}$ is the product of interface area $|\Gamma_{ij}|$ and interface normal vector $\boldsymbol{n}_{ij}$ (see figure 1). In other words, FVPM is very similar to FVM – only grid generation is replaced by integration. From the update rule in (8) it is clear that the value u_i at particle i is only influenced by those values u_j for which $\boldsymbol{\beta}_{ij} \neq 0$. In view of (7), this can only happen if the particles i and j overlap. Hence, it is natural to call ψ_i and ψ_j (interacting) neighbors if $\boldsymbol{\beta}_{ij} \neq 0$. In particular, the sum in (8) only involves the particles from the neighbor list $N_i = \{j : \boldsymbol{\beta}_{ij} \neq 0\}$. Note also that particle i does not interact with itself since $\boldsymbol{\beta}_{ii} = 0$ according to (7).

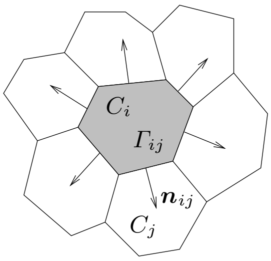

Fig. 1. Control volume C_i with interfaces Γ_{ij} and outer normals $\boldsymbol{n}_{ij}$

Before investigating the scheme (8) more closely, let us remark that the derivation works similarly in the case when the partition of unity is time dependent (moving particles). For simplicity, we assume here that the time dependence is such that ψ_i satisfy the advection equation

$$\frac{\partial \psi_i}{\partial t} + \boldsymbol{a} \cdot \nabla \psi_i = 0 \tag{9}$$

where $\boldsymbol{a}$ is a smooth and bounded velocity field. Note that $\{\psi_i(t, \cdot)\}_{i \in I}$ is automatically a partition of unity if this is true initially. However, the parameters

V_i and $\boldsymbol{\beta}_{ij}$ now depend on time. If we use these functions ψ_i as test functions, the time derivative gives rise to an additional term

$$\int_{\mathbb{R}^d} \psi_i \left(\frac{\partial u}{\partial t} + \operatorname{div} \boldsymbol{F}(u) \right) d\boldsymbol{x} = \frac{d}{dt} \int_{\mathbb{R}^d} \psi_i u \, d\boldsymbol{x} - \int_{\mathbb{R}^d} (\boldsymbol{F}(u) - u\boldsymbol{a}) \cdot \nabla \psi_i \, d\boldsymbol{x}$$

which is of the same form as (4) if $\boldsymbol{F}(u)$ is replaced by the *Lagrangian flux* $\boldsymbol{G}(t, \boldsymbol{x}, u) = \boldsymbol{F}(u) - u\boldsymbol{a}(t, \boldsymbol{x})$. Another possibility to generate a time dependent partition of unity is to move the points $\boldsymbol{x}_i$ according to the vector field $\boldsymbol{a}$ and to continuously apply Shephard's method to $W_i(\boldsymbol{x}) = W((\boldsymbol{x} - \boldsymbol{x}_i)/h)$. Also in this case, the modifications can be incorporated into the flux function by going over from $\boldsymbol{F}$ to $\boldsymbol{G}$ (for details, we refer to [11]).

In the following, we study mathematical properties of the Finite Volume Particle Method. For numerical results, we refer to [7, 12, 24, 31].

2.2 Geometric parameters

Inspecting the convergence proof for classical Finite Volume schemes (e.g. [1, 3, 14, 29]), one observes that there are only a few requirements on the geometric parameters $\boldsymbol{\beta}_{ij}, V_i$: the number of cell faces should be bounded, the cell surface area $\sum_j |\boldsymbol{\beta}_{ij}|$ should be of the order h^{d-1}, and the cell volumes V_i should be bounded from below by αh^d. Moreover, there are two important algebraic requirements. The first one reflects the fact that, if two cells C_i, C_j share a common interface, then the surface area $|\boldsymbol{\beta}_{ij}| = |\boldsymbol{\beta}_{ji}|$ is equal but the orientation $\boldsymbol{\beta}_{ij}/|\boldsymbol{\beta}_{ij}| = -\boldsymbol{\beta}_{ji}/|\boldsymbol{\beta}_{ji}|$ is opposite. The second requirement is related to the divergence theorem. If $\boldsymbol{\beta}_{ij}$ is the product of interface area and interface normal, then the sum $\sum_j \boldsymbol{\beta}_{ij}$ is nothing but the integral of the normal vector over the surface of cell C_i. According to the divergence theorem, this surface integral can be written as a volume integral of the divergence of constant fields so that $\sum_j \boldsymbol{\beta}_{ij} = 0$.

In the following, we show that the same conditions are satisfied if the geometric parameters $\boldsymbol{\beta}_{ij}, V_i$ are *not* based on a mesh but are obtained by integration from a partition of unity. As a consequence, many aspects of convergence proofs for classical Finite Volume schemes can be taken over without modification (examples are given in the following section). We start by a precise statement of our assumptions concerning the partition of unity.

(P1) *The initial partition of unity is constructed according to* (2), (3)*, based on a locally finite point distribution* $\{\boldsymbol{x}_i\}$*. We assume that the maximal number of overlapping particles is bounded, i.e.*

$$\max_{i \in I} \#\{j : \operatorname{supp} W_i \cap \operatorname{supp} W_j \neq \emptyset\} = K < \infty. \tag{10}$$

Moreover, there should be a minimal overlap such that

$$\sum_{i \in I} W_i(\boldsymbol{x}) \geq \mu > 0 \qquad \forall \boldsymbol{x} \in \mathbb{R}^d. \tag{11}$$

If we consider a sequence of partitions based on $W_i^h(\boldsymbol{x}) = W((\boldsymbol{x}-\boldsymbol{x}_i^h)/h)$ *with* $h \to 0$*, we assume that* K *and* μ *are* h*-independent.*
(P2) *The functions* $\psi_i(t,\cdot)$*,* $t > 0$ *are obtained by solving* (9) *with initial values given by the functions of the initial partition. The field* $\boldsymbol{a}$ *is assumed to be bounded and continuously differentiable with bounded derivatives.*

Using standard results from the theory of ordinary differential equations, we conclude that the initial value problem $\dot{\boldsymbol{x}}(t) = \boldsymbol{a}(t, \boldsymbol{x}(t))$, $\boldsymbol{x}(\tau) = \boldsymbol{\xi}$ admits a unique global solution which we denote by $t \to \boldsymbol{X}(t, \boldsymbol{\xi}, \tau)$. The function $\boldsymbol{X}$ is smooth and invertible with respect to the $\boldsymbol{\xi}$-variable, where

$$\boldsymbol{X}(t, \boldsymbol{X}(\tau, \boldsymbol{y}, t), \tau) = \boldsymbol{y} \qquad \forall \boldsymbol{y} \in \mathbb{R}^d.$$

The Jacobian determinant of $\boldsymbol{X}(t, \boldsymbol{\xi}, \tau)$ is given by

$$J(t, \boldsymbol{\xi}, \tau) = \exp\left(\int_\tau^t (\operatorname{div}\boldsymbol{a})(s, \boldsymbol{X}(s, \boldsymbol{\xi}, \tau))\, ds\right).$$

According to the method of characteristics, the solution of (9) satisfies

$$\psi_i(t, \boldsymbol{x}) = \psi(0, \boldsymbol{X}(0, \boldsymbol{x}, t)) \tag{12}$$

which immediately implies that $\{\psi_i(t,\cdot)\}_{i\in I}$ is a partition of unity. We want to stress again that the restriction to the construction (9) is not compulsory. It only helps us to avoid additional technical arguments and assumptions which are necessary, for example, if we use moving points $\boldsymbol{x}_i$ and construct the partition from the functions W_i which have moving supports of fixed shape. Also in that more technical situation, the following result can be shown.

Proposition 1. *Assume (P1) and (P2) and let* $V_i(t), \boldsymbol{\beta}_{ij}(t)$ *be defined by* (6) *and* (7) *based on the partition functions* $\{\psi_i(t,\cdot)\}_{i\in I}$*. Then there exist constants* $\alpha, K, C > 0$ *such that for* $t \in [0,T]$ *the number of neighbors is bounded* $\#N_i(t) \le K$ *and*

$$V_i(t) \ge \alpha h^d, \qquad \sum_j |\boldsymbol{\beta}_{ij}| \le C h^{d-1}. \tag{13}$$

Moreover, the relations

$$\boldsymbol{\beta}_{ij} = -\boldsymbol{\beta}_{ji}, \qquad \sum_j \boldsymbol{\beta}_{ij} = 0, \qquad i,j \in I \tag{14}$$

are satisfied.

Proof. The algebraic conditions (14) follow directly from the skew-symmetric definition of $\boldsymbol{\beta}_{ij}$. The vanishing sum over $\boldsymbol{\beta}_{ij}$ is a consequence of the fact that $\sum_j \psi_j = 1$, and $\int \nabla\psi_i \, d\boldsymbol{x} = \boldsymbol{0}$

$$\sum_j \boldsymbol{\beta}_{ij} = \int_{\mathbb{R}^d} \psi_i \nabla \sum_j \psi_j \, d\boldsymbol{x} - \int_{\mathbb{R}^d} \nabla\psi_i \, d\boldsymbol{x} = 0.$$

While these arguments do not depend on the structure of the partition, the estimates (13) require more details. We begin with the investigation of the volume.

$$V_i(t) = \int_{\mathbb{R}^d} \psi_i(t,\boldsymbol{x})\,d\boldsymbol{x} = \int_{\mathbb{R}^d} \psi_i(t,\boldsymbol{X}(0,\boldsymbol{x},t))\,d\boldsymbol{x} = \int_{\mathbb{R}^d} \psi_i(t,\boldsymbol{y})J(t,\boldsymbol{y},0)\,d\boldsymbol{y}.$$

If m is a lower bound for div$\boldsymbol{a}$, then $J(t,\boldsymbol{y},0) \geq \exp(tm)$ and it suffices to estimate $\psi_i(0,\boldsymbol{y}) = \psi_i^0(\boldsymbol{y})$ from below. In view of (10) and (12), the maximal number of overlapping particles is K (which also proves the estimate of $\#N_i$) and in connection with (11), we conclude

$$\mu \leq \sigma(\boldsymbol{y}) = \sum_k W_k(\boldsymbol{y}) \leq K\|W\|_\infty, \qquad \forall \boldsymbol{y} \in \mathbb{R}^d. \tag{15}$$

Continuing the estimate of V_i, we have

$$V_i(t) \geq \exp(tm) \int_{\mathbb{R}^d} \frac{W_i(\boldsymbol{y})}{\sigma(\boldsymbol{y})}\,d\boldsymbol{y} \geq \frac{\exp(Tm)}{K\|W\|_\infty} h^d \int_{\mathbb{R}^d} W(\boldsymbol{z})\,d\boldsymbol{z} = \alpha h^d$$

Next, we turn to the estimate of the sum over $|\boldsymbol{\beta}_{ij}|$. Allying integration by parts to (7), we have $\boldsymbol{\beta}_{ij} = 2\int \psi_j \nabla\psi_i\,d\boldsymbol{x}$, so that

$$\sum_j |\boldsymbol{\beta}_{ij}| \leq 2\int_{\mathbb{R}^d} |\nabla\psi_i|\,d\boldsymbol{x} \leq 2\int_{\mathbb{R}^d} |\nabla\psi_i|\,d\boldsymbol{x}.$$

Using chain rule and the same change of coordinates as above, we obtain

$$\sum_j |\boldsymbol{\beta}_{ij}| \leq 2\int_{\mathbb{R}^d} |(\nabla\boldsymbol{X})^T|\,|\nabla\psi_i^0| J\,d\boldsymbol{y}.$$

Gronwall's lemma implies that the derivatives of $\boldsymbol{X}$ can be bounded in terms of the derivatives of $\boldsymbol{a}$. If $|\nabla\boldsymbol{a}| \leq M$ then $|(\nabla\boldsymbol{X})^T| \leq \exp(tM)$ and $J \leq \exp(tMd)$. Hence, it suffices to estimate the integral over $|\nabla\psi_i^0|$. Definition (3) implies

$$\nabla\psi_i^0 = \frac{\nabla W_i}{\sigma} - \psi_i \frac{\sum_k \nabla W_k}{\sigma},$$

so that with (15)

$$\int_{\mathbb{R}^d} |\nabla\psi_i^0|\,d\boldsymbol{y} \leq \frac{2}{h\mu}\int_{\mathbb{R}^d} |\nabla W|(\boldsymbol{y}/h)\,d\boldsymbol{y} = \frac{2}{\mu}h^{d-1}\int_{\mathbb{R}^d} |\nabla W(\boldsymbol{z})|\,d\boldsymbol{z}$$

and hence

$$\sum_j |\boldsymbol{\beta}_{ij}| \leq \exp((d+1)TM)\frac{2(K+1)}{\mu}h^{d-1}.$$

This completes the proof. □

2.3 Stability

The aim of this section is to demonstrate that local averages u_i^n generated with FVPM can be estimated in the same way as in the mesh based Finite Volume approach. Our main assumption is that the flux function g is monotone. Note, however, that we allow for moving particles so that g should be an approximation of the Lagrangian flux $\boldsymbol{F}(u) - u\boldsymbol{a}(t, \boldsymbol{x})$. Consequently, the flux between two particles will also depend on their location and time. Since the dependence on location can be introduced in several ways (see below), we do not specify it at this stage. More precisely, we incorporate the possible movement of the particles into (8) by assuming the form

$$u_i^{n+1} V_i^{n+1} = u_i^n V_i^n - \Delta t \sum_j G_{ij}^n(u_i^n, u_j^n) \tag{16}$$

with initial values

$$u_i^0 = \frac{1}{V_i^0} \int_{\mathbb{R}^d} u^0(\boldsymbol{x}) \psi(0, \boldsymbol{x})\, d\boldsymbol{x}.$$

where the flux function G_{ij}^n should satisfy the following requirements.

(Z) Local interaction is ensured by

$$G_{ij}^n(u, v) = 0 \qquad \text{for } j \notin N_i^n.$$

(S) The flux function should be antisymmetric in the following sense

$$G_{ij}^n(u, v) = -G_{ji}^n(v, u).$$

(C) The relation to the Lagrangian flux is ensured by

$$G_{ij}^n(u, u) = \boldsymbol{F}(u) \cdot \boldsymbol{\beta}_{ij}^n - u \boldsymbol{A}_{ij}^n \cdot \boldsymbol{\beta}_{ij}^n$$

where $\boldsymbol{A}_{ij}^n$ approximates $\boldsymbol{a}$ on the support of ψ_i

$$|\boldsymbol{A}_{ij}^n - \boldsymbol{a}(t_n, \boldsymbol{x}_i^n)| \leq ch, \qquad j \in N_i^n \tag{17}$$

where $\boldsymbol{x}_i^n$ is the barycenter of particle i

$$\boldsymbol{x}_i^n = \frac{1}{V_i^n} \int_{\mathbb{R}^d} \boldsymbol{x} \psi(t_n, \boldsymbol{x})\, d\boldsymbol{x}.$$

(L) The flux function should be locally Lipschitz continuous, i.e. for $a \leq u, v, w \leq b$ we assume

$$|G_{ij}^n(u, w) - G_{ij}^n(v, w)| \leq |\boldsymbol{\beta}_{ij}| L(a, b) |u - v|.$$

(M) Finally, we assume monotonicity in the arguments of G_{ij}^n. For $u \neq v$

$$\frac{G_{ij}^n(u, w) - G_{ij}^n(v, w)}{u - v} \geq 0, \qquad \frac{G_{ij}^n(w, u) - G_{ij}^n(w, v)}{u - v} \leq 0.$$

In order to prove a conservation property of (16) we assume that the flux $\boldsymbol{F}(u)$ in (1) is defined for $u = 0$ (which can always be achieved by a simple transformation).

Proposition 2. *Assume (Z), (S), (C). If the initial value* u^0 *of* (1) *has a compact support then* $u_i^n \neq 0$ *for only finitely many indices* i *and*

$$\sum_i u_i^{n+1} V_i^{n+1} = \sum_i u_i^n V_i^n.$$

Proof. According to (P1), the point distribution $\{\boldsymbol{x}_i\}$ is locally finite which implies that the number of particles $\psi_i(0,\cdot)$ whose support intersect with the one of u^0 is finite. In particular, only finitely many average values u_i^0 are non-zero and the sum $\sum_i u_i^0 V_i^0$ is well defined. Considering a particle i with vanishing average $u_i^0 = 0$ and also $u_j^0 = 0$ for all neighbors $j \in N_i^0$, we have

$$u_i^1 V_i^1 = -\Delta t \sum_j G_{ij}^0(0,0) = -\Delta t \sum_j \left(\boldsymbol{F}(0) \cdot \boldsymbol{\beta}_{ij}^n - 0 \cdot \boldsymbol{A}_{ij}^n \cdot \boldsymbol{\beta}_{ij}^n \right)$$

where (C) has been used. Since the sum over $\boldsymbol{\beta}_{ij}$ vanishes according to (14), we see that $u_i^1 = 0$. This situation occurs for all but finitely many particles and hence $u_i^1 \neq 0$ only finitely often so that $\sum_i u_i^1 V_i^1$ is well defined. Summing over (16), we get

$$\begin{aligned}\sum_i u_i^1 V_i^1 - \sum_i u_i^0 V_i^0 &= -\Delta t \sum_{i,j} G_{ij}^0(u_i^0, u_j^0) \\ &= -\Delta t \left(\frac{1}{2} \sum_{i,j} G_{ij}^0(u_i^0, u_j^0) + \frac{1}{2} \sum_{j,i} G_{ji}^0(u_j^0, u_i^0) \right).\end{aligned}$$

Using (S), we conclude that the right hand side vanishes which yields conservation. Using an induction argument, the general statement follows. □

The second important property is monotonicity of the scheme.

Proposition 3. *Assume (L), (M) and let* $a \leq u_i^n, w_i^n \leq b$. *If for some* $\xi \in (0,1)$ *the CFL condition*

$$\Delta t \leq \min_{i \in I} \frac{\xi V_i^n}{L(a,b) \sum_j |\boldsymbol{\beta}_{ij}|}$$

is satisfied then $u_i^{n+1} \leq w_i^{n+1}$.

Proof. Assuming first that $u_i^n \neq w_i^n$, we obtain from (16)

$$\begin{aligned}(w_i^{n+1} - u_i^{n+1}) V_i^{n+1} &= -\Delta t \sum_j \left(G_{ij}^n(u_i^n, w_j^n) - G_{ij}^n(u_i^n, u_j^n) \right) \\ &+ \left(V_i^n - \Delta t \sum_j \frac{G_{ij}^n(w_i^n, w_j^n) - G_{ij}^n(u_i^n, w_j^n)}{w_i^n - u_i^n} \right) (w_i^n - u_i^n) \quad (18)\end{aligned}$$

Using the Lipschitz property

$$V_i^n - \Delta t \sum_j \frac{G_{ij}^n(w_i^n, w_j^n) - G_{ij}^n(u_i^n, w_j^n)}{w_i^n - u_i^n} \geq V_i^n \left(1 - \frac{\Delta t}{V_i^n} \sum_j |\boldsymbol{\beta}_{ij}| L(a,b)\right)$$

so that the second term on the right of (18) is positive if the CFL condition is satisfied. The positivity of the first term follows immediately from (M). In the case $u_i^n = w_i^n$, the second term is not present and non-negativity follows from the first term, again with the help of (M). □

An immediate consequence of monotonicity is $\mathbb{L}^\infty$-stability. Due to the possible movement of the particles, however, the maximum may increase in time.

Proposition 4. *There exist h-independent constants γ_1, γ_2 such that under the assumptions of Proposition 2 together with (C) and the additional restriction $\Delta t \leq \alpha/(2cC)$, where α, C are from* (13) *and c from* (17)*, we have*

$$\begin{aligned}
&\max_{i\in I} u_i^{n+1} \leq \exp(\gamma_1 \Delta t) \max_{i\in I} u_i^n && \textit{if } \max_i u_i^n \geq 0,\\
&\min_{i\in I} u_i^{n+1} \leq \exp(\gamma_1 \Delta t) \min_{i\in I} u_i^n && \textit{if } \min_i u_i^n \leq 0,\\
&\max_{i\in I} u_i^{n+1} \leq \exp(\gamma_2 \Delta t) \max_{i\in I} u_i^n && \textit{if } \max_i u_i^n \leq 0,\\
&\min_{i\in I} u_i^{n+1} \leq \exp(\gamma_2 \Delta t) \min_{i\in I} u_i^n && \textit{if } \min_i u_i^n \geq 0.
\end{aligned}$$

Proof. Using Proposition 2 with $w_i^n = \max_j u_j^n = M \geq 0$, we obtain $u_i^{n+1} \leq w_i^{n+1}$ which yields the desired estimate if $w_i^{n+1} \leq \exp(\gamma_1 \Delta t) M$. Since $w_i^n = M$, we obtain with (C)

$$\begin{aligned}
w_i^{n+1} V_i^{n+1} &= M V_i^n - \Delta t \sum_j \left(\boldsymbol{F}(M) \cdot \boldsymbol{\beta}_{ij}^n - M \boldsymbol{A}_{ij}^n \cdot \boldsymbol{\beta}_{ij}^n\right)\\
&= V_i^n \left(1 - \frac{\Delta t}{V_i^n} \sum_j \boldsymbol{A}_{ij}^n \cdot \boldsymbol{\beta}_{ij}^n\right) M.
\end{aligned}$$

The extra information about $\boldsymbol{A}_{ij}^n$ in (C) implies

$$\frac{\Delta t}{V_i^n} \left|\sum_j \boldsymbol{A}_{ij}^n \cdot \boldsymbol{\beta}_{ij}^n\right| \leq \frac{\Delta t}{V_i^n} \left|\sum_j \boldsymbol{a}(t_n, \boldsymbol{x}_i^n) \cdot \boldsymbol{\beta}_{ij}^n\right| + \frac{\Delta t}{V_i^n} ch \sum_j |\boldsymbol{\beta}_{ij}^n|$$

where the first term on the right vanishes because of (14). We conclude with (13)

$$\frac{\Delta t}{V_i^n} \left|\sum_j \boldsymbol{A}_{ij}^n \cdot \boldsymbol{\beta}_{ij}^n\right| \leq \frac{cC}{\alpha} \Delta t.$$

Due to the movement of the particles, $\psi_i(t_{n+1}, \boldsymbol{x}) = \psi_i(t_n, \boldsymbol{X}(t_n, \boldsymbol{x}, t_{n+1})$ and since the Jacobian determinant follows the estimate $J(t_{n+1}, bfy, t_n) \geq \exp(\delta \Delta t)$ with δ being the minimum of div$\boldsymbol{a}$, we have

$$V_i^{n+1} = \int_{\mathbb{R}^d} \psi_i(t_n, \boldsymbol{y}) J(t_{n+1}, \boldsymbol{y}, t_n)\, d\boldsymbol{y} \geq \exp(\delta \Delta t) V_i^n .$$

Combining these results and setting $\gamma_1 = cC/\alpha - \delta$, we finally get $w_i^{n+1} \leq \exp(\gamma_1 \Delta t) M$. Similarly, we can estimate the behavior of the minimum $m = \min_i u_i^n \geq 0$. Setting $w_i^n = m$, we conclude from $u_i^n \geq w_i^n$ that also $u_i^{n+1} \geq w_i^{n+1}$, and as above,

$$w_i^{n+1} \geq \left(1 - \frac{cC}{\alpha} \Delta t\right) \exp(\delta \Delta t) m.$$

Setting $D = \alpha/(2cC)$, we obtain $1 - \Delta t/(2D) \geq \exp(-\ln(2)\Delta t/D)$ for $0 \leq \Delta t \leq D$ so that the result follows with $\gamma_2 = \delta - \ln(2)/D$. The remaining cases where maximum or minimum are negative can be shown in the same way. □.

We remark that *no* exponential factors appear in the estimates for maximum and minimum if the volumes are *approximately* calculated from the formula

$$V_i^{n+1} = V_1^n \left(1 + \frac{\Delta t}{V_i^n} \sum_j \boldsymbol{A}_{ij}^n \cdot \boldsymbol{\beta}_{ij}^n \right).$$

This is an approximation to the true volume evolution because the sum over $\boldsymbol{A}_{ij}^n \cdot \boldsymbol{\beta}_{ij}^n$ can be regarded as approximation of div$\boldsymbol{a}$ if $\boldsymbol{A}_{ij}^n$ is an evaluation of $\boldsymbol{a}$ at a suitable point $\boldsymbol{x}_{ij}^n$ (see [12] for details).

Apart from $\mathbb{L}^\infty$-estimates, the monotonicity can also be used to derive a discrete Krushkov-entropy estimate. Moreover, a weak BV-estimate can be shown along the lines of the proof in [1]. We will not go into further details here but conclude with some comments on the construction of the flux function G_{ij}^n. A particular example is based on the Lax-Friedrichs flux function

$$G_{ij}^n(u,v) = \frac{\boldsymbol{F}(u) + \boldsymbol{F}(v)}{2} \cdot \boldsymbol{\beta}_{ij}^n + \frac{u-v}{2\lambda} - \frac{u}{2} \boldsymbol{a}(t_n, \boldsymbol{x}_i^n) \cdot \boldsymbol{\beta}_{ij}^n - \frac{v}{2} \boldsymbol{a}(t_n, \boldsymbol{x}_j^n) \cdot \boldsymbol{\beta}_{ij}^n \quad (19)$$

where $\boldsymbol{x}_i^n$, $\boldsymbol{x}_j^n$ are, for example, the barycenters of particles i and j at time t_n. If $\boldsymbol{F}$ is locally Lipschitz continuous and if the parameter λ is chosen such that $\lambda |\boldsymbol{F}'(u) - \boldsymbol{a}(t, \boldsymbol{x})| \leq 1$ for $a \leq u \leq b$, $t \in [0,T]$, and $\boldsymbol{x} \in \mathbb{R}^d$, then definition (19) satisfies the requirements (Z), (S), (C), (L), (M).

More generally, if $g_0(u, v, \boldsymbol{n})$ is any monotone and locally Lipschitz continuous numerical flux function which is consistent to $\boldsymbol{F}$, then

$$G_{ij}^n(u,v) = |\boldsymbol{\beta}_{ij}^n| g_0(u, v, \boldsymbol{n}_{ij}^n) + \left(u \frac{M - \boldsymbol{a}(t_n, \boldsymbol{x}_i^n)}{2} - v \frac{M + \boldsymbol{a}(t_n, \boldsymbol{x}_j^n)}{2}\right) \cdot \boldsymbol{\beta}_{ij}^n$$

satisfies all the requirements on the numerical flux function if $M \geq |\boldsymbol{a}(t, \boldsymbol{x})|$ for any $t \in [0,T]$, and $\boldsymbol{x} \in \mathbb{R}^d$. Instead of using two separate points, one can also base the construction on a common point $\boldsymbol{x}_{ij}^n$ for each pair of particles such that $\boldsymbol{x}_{ij}^n = \boldsymbol{x}_{ji}^n$ which replaces $\boldsymbol{x}_i^n$ and $\boldsymbol{x}_j^n$ in the construction above.

We close with the remark that a full convergence proof of the scheme (16) does *not* automatically follow from the estimates of the local averages u_i^n. This is due to the fact that the reconstruction of an approximate solution u_h from the discrete values is not so straightforward as in the classical Finite Volume case, where one sets

$$u_h(t, \boldsymbol{x}) = \sum_{i \in I} u_i^n \mathbf{1}_{C_i}(\boldsymbol{x}) \mathbf{1}_{[t_n, t_{n+1})}(t). \tag{20}$$

The intuitive choice

$$u_h(t, \boldsymbol{x}) = \sum_{i \in I} u_i^n \psi_i(\boldsymbol{x}) \mathbf{1}_{[t_n, t_{n+1})}(t) \tag{21}$$

seems to be promising because u_h is bounded in $\mathbb{L}^\infty$ by the maximum of $|u_i^n|$ and the reconstruction is conservative

$$\int_{\mathbb{R}^d} u_h(t_n, \boldsymbol{x})\, d\boldsymbol{x} = \sum_i u_i^n V_i^n = \sum_i u_i^0 V_i^0 = \int_{\mathbb{R}^d} u^0(\boldsymbol{x})\, d\boldsymbol{x}$$

(although locally $\int u_h(t_n, \boldsymbol{x}) \psi_i(t_n, \boldsymbol{x})\, d\boldsymbol{x} \neq u_i^n V_i^n$, in general). The main difficulty with the reconstruction (21) in the convergence proof is that it does not commute with nonlinear functions. While in the FV approach (20) the flux of the reconstruction is equal to the reconstruction of the fluxes,

$$\boldsymbol{F}(u_h(t, \boldsymbol{x})) = \sum_{i \in I} \boldsymbol{F}(u_i^n) \mathbf{1}_{C_i}(\boldsymbol{x}) \mathbf{1}_{[t_n, t_{n+1})}(t),$$

a similar relation is not available for the reconstruction (21). Therefore, the estimates in terms of u_i^n cannot immediately be used for the reconstruction and further analysis is required for a complete convergence proof.

3 The Finite Pointset Method

As we have seen in section 2.1, the Finite Volume Particle Method can be interpreted as a discretization of the *weak* form of conservation laws. The only difference to the classical Finite Volume Method is that the test functions are not constructed from mesh cells but are chosen as smooth partition of unity functions. The flux-divergence div$\boldsymbol{F}$ is approximated with the help of geometric parameters which depend on the relative location of the particles (similar to the classical Finite Volume Method where div$\boldsymbol{F}$ is replaced by an approximate surface integral over the flux – reflecting the weak formulation). While the weak approximation has the advantage of ensuring discrete conservation and stability, it also requires a large numerical effort for the evaluation of the geometric parameters and is, in its basic form, of low approximation order.

In the Finite Pointset Method (FPM) these advantages and disadvantages are essentially reversed. The method is based on the *strong* form of the equation and therefore has the basic flavor of a Finite Difference scheme. Derivatives are approximated using a least squares approach which requires only little information about the relative location of the particles and easily allows high order approximations. However, as a consequence of the higher geometrical flexibility, discrete conservation cannot be proved (there is no volume associated to the particles and therefore integral values are not defined as naturally as in the Finite Volume approach), and also stability estimates are not available through standard techniques, eventhough the method has been successfully applied to a wide variety of problems.

In the following, we describe the adaption of the method to the case of incompressible, viscous, multiphase flows.

3.1 Mathematical model and numerical scheme

We consider two immiscible fluids, for example, liquid and gas in a situation where the motion can be described by the incompressible Navier-Stokes equations. They are, in Lagrangian form,

$$\frac{D\boldsymbol{v}}{Dt} = -\frac{1}{\rho}\nabla p + \frac{1}{\rho}\nabla \cdot (2\mu D) + \boldsymbol{g}, \tag{22}$$

$$\nabla \cdot \boldsymbol{v} = 0 \tag{23}$$

where $\boldsymbol{v}$ is the fluid velocity vector, ρ is the fluid density, μ is the fluid viscosity, D is the viscous stress tensor $D = \frac{1}{2}(\nabla \boldsymbol{v} + \nabla^T \boldsymbol{v})$ and $\boldsymbol{g}$ is the body force acceleration vector.

For a numerical simulation of the process, we assume that the flow domain is filled by a set of discretization points (point cloud). Each point (also referred to as particle) locally represents a lump of fluid. The points carry all necessary pieces of information (state variables) in order to completely describe the local state of flow, such as density, velocity, pressure, etc. The particles move exactly with fluid velocity, and, of course, the task of the numerical scheme is to evolve the state variables at the particle locations in an accurate way. The point cloud itself may be locally adaptive, i.e. the mean distance between points may change locally due to certain criteria. That also means that, during computation, new particles have to be created in sparse regions and removed in dense areas.

In this paper, we initially provide each particle a flag representing the fluid phase it belongs to. These flags do not change throughout the computation. Moreover, the density and viscosity are constant on each particle path, so we have

$$\frac{\partial \rho}{\partial t} + \boldsymbol{v} \cdot \nabla \rho = 0 \tag{24}$$

$$\frac{\partial \mu}{\partial t} + \boldsymbol{v} \cdot \nabla \mu = 0. \tag{25}$$

Therefore, each fluid particle has constant ρ and μ. Since ρ and μ are discontinuous across the interface, the numerical scheme might have instabilities in that particular region. Therefore, we consider a smooth density and viscosity in the vicinity of an interface. The interface region can be detected by checking the flags of particles in the neighborhood. If there are flags of only one type in the neighbor list of some particle, then it is considered to be far from the interface region. Near the interface, particles will find both types of flags in the neighbor list. We modify the density and viscosity in each time step at each particle position $\boldsymbol{x}$ near the interface by using the Shepard interpolation

$$\tilde{\rho}(\boldsymbol{x}) = \frac{\sum_{i=1}^{n} w_i \rho_i}{\sum_{i=1}^{n} w_i} \tag{26}$$

$$\tilde{\mu}(\boldsymbol{x}) = \frac{\sum_{i=1}^{n} w_i \mu_i}{\sum_{i=1}^{n} w_i}, \tag{27}$$

where n is the total number of neighbor particles $\boldsymbol{x}_i$ at $\boldsymbol{x}$ inside the compact support of the weight function w_i which is defined by (38). Occasionally, the smoothing procedure of density and viscosity has to be repeated several times in order to gain stability. Equations (22–23) are solved togehter with some initial and boundary conditions.

Numerical scheme

Since the viscosity is smoothed near the interface, we can rewrite the momentum equations whose spatial components are given by

$$\frac{du}{dt} = g_x - \frac{1}{\tilde{\rho}}\frac{\partial p}{\partial x} + \frac{1}{\tilde{\rho}}\nabla\tilde{\mu}\cdot\nabla u + \frac{\tilde{\mu}}{\tilde{\rho}}\Delta u + \frac{1}{\tilde{\rho}}(\frac{\partial\tilde{\mu}}{\partial x}\frac{\partial u}{\partial x} + \frac{\partial\tilde{\mu}}{\partial y}\frac{\partial v}{\partial x} + \frac{\partial\tilde{\mu}}{\partial z}\frac{\partial w}{\partial x})$$

$$\frac{dv}{dt} = g_y - \frac{1}{\tilde{\rho}}\frac{\partial p}{\partial y} + \frac{1}{\tilde{\rho}}\nabla\tilde{\mu}\cdot\nabla v + \frac{\tilde{\mu}}{\tilde{\rho}}\Delta v + \frac{1}{\tilde{\rho}}(\frac{\partial\tilde{\mu}}{\partial x}\frac{\partial u}{\partial y} + \frac{\partial\tilde{\mu}}{\partial y}\frac{\partial v}{\partial y} + \frac{\partial\tilde{\mu}}{\partial z}\frac{\partial w}{\partial y})$$

$$\frac{dw}{dt} = g_x - \frac{1}{\tilde{\rho}}\frac{\partial p}{\partial z} + \frac{1}{\tilde{\rho}}\nabla\tilde{\mu}\cdot\nabla w + \frac{\tilde{\mu}}{\tilde{\rho}}\Delta w + \frac{1}{\tilde{\rho}}(\frac{\partial\tilde{\mu}}{\partial x}\frac{\partial u}{\partial z} + \frac{\partial\tilde{\mu}}{\partial y}\frac{\partial v}{\partial z} + \frac{\partial\tilde{\mu}}{\partial z}\frac{\partial w}{\partial z}).$$

To ensure incompressibility, we use Chorin's projection method [2]. Since we consider the fully Lagrangian method, we first move particles with their old velocities. The new positions are given by

$$\boldsymbol{x}^{n+1} = \boldsymbol{x}^n + \Delta t\ \boldsymbol{v}^n.$$

At each new particle position we modify the density and viscosity according to (26) and (27), respectively and then compute the intermediate velocities u^*, v^* and w^* implicitly by

$$u^* - \frac{\Delta t}{\tilde{\rho}}(\nabla\tilde{\mu}\cdot\nabla u^* - \tilde{\mu}\Delta u^*) = u^n + \Delta t\, g_x + \frac{\Delta t}{\tilde{\rho}}\,\nabla\tilde{\mu}\cdot\frac{\partial \boldsymbol{v}^n}{\partial x} \qquad (28)$$

$$v^* - \frac{\Delta t}{\tilde{\rho}}(\nabla\tilde{\mu}\cdot\nabla v^* - \tilde{\mu}\Delta v^*) = v^n + \Delta t\, g_y + \frac{\Delta t}{\tilde{\rho}}\,\nabla\tilde{\mu}\cdot\frac{\partial \boldsymbol{v}^n}{\partial y} \qquad (29)$$

$$w^* - \frac{\Delta t}{\tilde{\rho}}(\nabla\tilde{\mu}\cdot\nabla w^* - \tilde{\mu}\Delta w^*) = w^n + \Delta t\, g_z + \frac{\Delta t}{\tilde{\rho}}\,\nabla\tilde{\mu}\cdot\frac{\partial \boldsymbol{v}^n}{\partial z}. \qquad (30)$$

Then, at the second step, we correct $\boldsymbol{v}^* = (u^*, v^*, w^*)$ by solving the equation

$$\boldsymbol{v}^{n+1} = \boldsymbol{v}^* - \Delta t\,\frac{\nabla p^{n+1}}{\tilde{\rho}} \qquad (31)$$

for p^{n+1}, with the incompressibility constraint

$$\nabla\cdot\boldsymbol{v}^{n+1} = 0. \qquad (32)$$

By taking the divergence of equation (31) and by making use of (32), we obtain the Poisson equation for the pressure

$$\nabla\cdot\left(\frac{\nabla p^{n+1}}{\tilde{\rho}}\right) = \frac{\nabla\cdot\boldsymbol{v}^*}{\Delta t}. \qquad (33)$$

The boundary condition for p is obtained by projecting the equation (31) on the outward unit normal vector $\boldsymbol{n}$ to the boundary Γ. Thus, we obtain the Neumann boundary condition

$$\left(\frac{\partial p}{\partial \boldsymbol{n}}\right)^{n+1} = -\frac{\tilde{\rho}}{\Delta t}(\boldsymbol{v}_\Gamma^{n+1} - \boldsymbol{v}_\Gamma^*)\cdot\boldsymbol{n}, \qquad (34)$$

where $\boldsymbol{v}_\Gamma$ is the value of $\boldsymbol{v}$ on Γ. Assuming $\boldsymbol{v}\cdot\boldsymbol{n} = 0$ on Γ, we obtain

$$\left(\frac{\partial p}{\partial \boldsymbol{n}}\right)^{n+1} = 0 \qquad (35)$$

on Γ.

We note that particle positions change only in the first step. The intermediate velocity $\boldsymbol{v}^*$ is obtained on the new particle positions. The pressure Poisson equation and the divergence free velocity vector are also computed on the new particle positions.

We solve the above implicit equations (28–30) for the velocity vector $\boldsymbol{v}^*$ and pressure (33) by the constraint weighted least squares method which is described in the following section.

3.2 FPM for solving general elliptic partial differential equations

To generalize the pressure Poisson problem, we consider the following linear partial differential equation of second order

$$A\psi + \boldsymbol{B} \cdot \nabla\psi + C\Delta\psi = f, \tag{36}$$

where $A, \boldsymbol{B}, C$ and f are given. Note that for the pressure Poisson equation (33), we have $A = 0$. The equation is solved with Dirichlet or Neumann boundary conditions

$$\psi = g \qquad \text{or} \qquad \frac{\partial\psi}{\partial \boldsymbol{n}} = \phi. \tag{37}$$

We use the method proposed in [26] to solve the elliptic equation in a meshfree framework. According to [9], it is more stable than the approach presented in [17] and it easily handles Neumann boundary conditions.

Consider the computational domain $\Omega \in R^d, d \in \{1,2,3\}$. Distribute N particles $\boldsymbol{x}_j \in \Omega, j = 1, \cdots, N$, which are the discretization points and might be irregular. Let $\boldsymbol{x}$ be an arbitrary particle in Ω, and we determine its neighboring cloud of points. We introduce the weight function $w = w(\boldsymbol{x}_i - \boldsymbol{x}, h)$ with small compact support of radius h. The weight function can be arbitrary but in our computation, we consider a Gaussian weight function of the following form

$$w(\boldsymbol{x}_i - \boldsymbol{x}; h) = \begin{cases} \exp(-\alpha \frac{\|\boldsymbol{x}_i - \boldsymbol{x}\|^2}{h^2}), & \text{if } \frac{\|\boldsymbol{x}_i - \boldsymbol{x}\|}{h} \leq 1 \\ 0, & \text{else,} \end{cases} \tag{38}$$

where α is a positive constant. Usually we choose $\alpha = 6.25$ but in case of Shepard interpolation $\alpha = 2$. The size of h defines a set of neighboring particles around $\boldsymbol{x}$. Let $P(\boldsymbol{x}, h) = \{\boldsymbol{x}_i : i = 1, 2, \ldots, m\}$ be the set of m neighboring points of $\boldsymbol{x}$ in a ball of radius h.

A basic idea in FPM is to construct approximate derivatives from point values using a least squares approach [15, 16, 25, 27, 28]. This leads to some obvious restrictions on the number and the location of points in $P(\boldsymbol{x}, h)$. Since we consider general second order equations, all derivatives up to order two (and the function value itself) should be constructable so that, in $3D$, a minimal requirement is that $P(\boldsymbol{x})$ contains at least ten points.

To explain the least squares approach, consider the Taylor expansions of $\psi(\boldsymbol{x}_i)$ around $\boldsymbol{x}$

$$\psi(\boldsymbol{x}_i) = \sum_{|j| \leq 2} \frac{\partial\psi^{|j|}}{\partial x^{j_1} \partial y^{j_2} \partial z^{j_3}} \, \frac{1}{j!} \, (x_i - x)^{j_1} (y_i - y)^{j_2} (z_i - z)^{j_3} + e_i, \tag{39}$$

for $i = 1, \ldots, m$, where e_i is the truncation error (we expand to second order for simplicity – higher order expansions are, of course, possible). Denote the coefficients

$$a_0 = \psi(\boldsymbol{x}), \qquad a_1 = \frac{\partial\psi}{\partial x}, \qquad a_2 = \frac{\partial\psi}{\partial y}, \qquad a_3 = \frac{\partial\psi}{\partial z}, \qquad a_4 = \frac{\partial^2\psi}{\partial x^2},$$

$$a_5 = \frac{\partial^2\psi}{\partial x \partial y}, \qquad a_6 = \frac{\partial^2\psi}{\partial x \partial z}, \qquad a_7 = \frac{\partial^2\psi}{\partial y^2}, \qquad a_8 = \frac{\partial^2\psi}{\partial y \partial z}, \qquad a_9 = \frac{\partial^2\psi}{\partial z^2}.$$

To the m equations (39) we add the equations (36) and (37) which are re-expressed as

$$\begin{aligned} Aa_0 + B_1a_1 + B_2a_2 + B_3a_3 + C(a_4 + a_7 + a_9) &= f \\ n_xa_1 + n_ya_2 + n_za_3 &= \phi, \end{aligned}$$

where n_x, n_y, n_z are the spatial components of the unit normal vector $\boldsymbol{n}$ on the boundary Γ.

Note that, for the Dirichlet boundary condition, we have only $m+1$ equations, where we directly prescribe the boundary conditions on the boundary particles.

Now, we have to solve $m+2$ equations. For $m+2 > 10$ this system is over-determined with respect to the unknowns a_i and can be written in matrix form as

$$\boldsymbol{e} = M\boldsymbol{a} - \boldsymbol{b},$$

where

$$M = \begin{pmatrix} 1 & h_{1,1} & h_{2,1} & h_{3,1} & \frac{1}{2}h_{1,1}^2 & h_{1,1}h_{2,1} & h_{1,1}h_{3,1} & \frac{1}{2}h_{2,1}^2 & h_{2,1}h_{3,1} & \frac{1}{2}h_{3,1}^2 \\ \vdots & \vdots & \vdots & \vdots & \vdots & \vdots & \vdots & \vdots & \vdots & \vdots \\ 1 & h_{1,m} & h_{2,m} & h_{3,m} & \frac{1}{2}h_{1,m}^2 & h_{1,m}h_{2,m} & h_{1,m}h_{3,m} & \frac{1}{2}h_{2,m}^2 & h_{2,m}h_{3,m} & \frac{1}{2}h_{3,m}^2 \\ A & B_1 & B_2 & B_3 & C & 0 & 0 & C & 0 & C \\ 0 & n_x & n_y & n_z & 0 & 0 & 0 & 0 & 0 & 0 \end{pmatrix},$$

$\boldsymbol{a} = (a_0, a_1, \ldots, a_9)^T$, $\boldsymbol{b} = (\psi_1, \ldots, \psi_m, f, g)^T$, $\boldsymbol{e} = (e_1, \ldots, e_m, e_{m+1}, e_{m+2})^T$ and $h_{1,i} = x_i - x,\ h_{2,i} = y_i - y,\ h_{3,i} = z_i - z$.

The unknowns $\boldsymbol{a}$ are computed by minimizing a weighted error over the neighboring points. Thus, we have to minimize the following quadratic form

$$J = \sum_{i=1}^{m+2} w_i e_i^2, \tag{40}$$

where $e_{m+1} = (A\psi + \boldsymbol{B} \cdot \nabla\psi + C\Delta\psi - f)$, $e_{m+2} = \left(\frac{\partial\psi}{\partial\boldsymbol{n}} - \phi\right)$ and the corresponding weights $w_{m+1} = w_{m+2} = 1$. The above equation (40) can be re-expressed in the form

$$J = (M\boldsymbol{a} - \boldsymbol{b})^T W (M\boldsymbol{a} - \boldsymbol{b})$$

with the diagonal matrix

$$W = diag\,(w_1, w_2, \ldots, w_m, 1, 1)\,.$$

The minimization of J with respect to $\boldsymbol{a}$ formally yields (if M^TWM is non-singular)

$$\boldsymbol{a} = (M^TWM)^{-1}(M^TW)\boldsymbol{b}. \tag{41}$$

In (41) the vector $(M^TW)\boldsymbol{b}$ is explicitly given by

$$\begin{aligned}(M^TW)\boldsymbol{b} = \Bigg(& \sum_{i=1}^{m} w_i\psi_i + Af,\ \sum_{i=1}^{m} w_i h_{1,i}\psi_i + B_1 f + n_x\phi, \\ & \sum_{i=1}^{m} w_i h_{2,i}\psi_i + B_2 f + n_y\phi,\ \sum_{i=1}^{m} w_i h_{3,i}\psi_i + B_3 f + n_z\phi, \\ & \frac{1}{2}\sum_{i=1}^{m} w_i h_{1,i}^2\psi_i + Cf,\ \sum_{i=1}^{m} w_i h_{1,i}h_{2,i}\psi_i,\ \sum_{i=1}^{m} w_i h_{1,i}h_{3,i}\psi_i, \\ & \frac{1}{2}\sum_{i=1}^{m} w_i h_{2,i}^2\psi_i + Cf,\ \sum_{i=1}^{m} w_i h_{2,i}h_{3,i}\psi_i,\ \frac{1}{2}\sum_{i=1}^{m} w_i h_{3,i}^2\psi_i + Cf\Bigg)^T .\end{aligned}$$

Thus we obtain from equation (41) that

$$\begin{aligned}\psi = {} & Q_{11}\left(\sum_{i=1}^{m} w_i\psi_i + Af\right) && + Q_{12}\left(\sum_{i=1}^{m} w_i h_{1,i}\psi_i + B_1 f + n_x\phi\right) \\ & + Q_{13}\left(\sum_{i=1}^{m} w_i h_{2,i}\psi_i + B_2 f + n_y\phi\right) && + Q_{14}\left(\sum_{i=1}^{m} w_i h_{3,i}\psi_i + B_3 f + n_z\phi\right) \\ & + Q_{15}\left(\frac{1}{2}\sum_{i=1}^{m} w_i h_{1,i}^2\psi_i + Cf\right) && + Q_{16}\left(\sum_{i=1}^{m} w_i h_{1,i}h_{2,i}\psi_i\right) \\ & + Q_{17}\left(\sum_{i=1}^{m} w_i h_{1,i}h_{3,i}\psi_i\right) && + Q_{18}\left(\frac{1}{2}\sum_{i=1}^{m} w_i h_{2,i}^2\psi_i + Cf\right) \\ & + Q_{19}\left(\sum_{i=1}^{m} w_i h_{2,i}h_{3,i}\psi_i\right) + && + Q_{1,10}\left(\frac{1}{2}\sum_{i=1}^{m} w_i h_{3,i}^2\psi_i + Cf\right),\end{aligned}$$

where $Q_{11}, Q_{12}, \ldots, Q_{1,10}$ is the first row of the matrix $(M^TWM)^{-1}$. Rearranging the terms, we have

$$\begin{aligned}\psi - \sum_{i=1}^{m} w_i \Bigg(& Q_{11} + Q_{12}h_{1,i} + Q_{13}h_{2,i} + Q_{14}h_{3,i} + Q_{15}\frac{h_{1,i}^2}{2} + \\ & Q_{16}h_{1,i}h_{2,i} + Q_{17}h_{1,i}h_{3,i} + Q_{18}\frac{h_{2,i}^2}{2} + Q_{19}h_{2,i}h_{3,i} + Q_{1,10}\frac{h_{3,i}^2}{2}\Bigg)\psi_i = \\ & \left(Q_{11}A + Q_{12}B_1 + Q_{13}B_2 + Q_{14}B_3 + Q_{15}C + Q_{18}C + Q_{1,10}C\right) f + \\ & \left(Q_{12}n_x + Q_{13}n_y + Q_{14}n_z\right)\phi.\end{aligned}$$

Hence, if $\boldsymbol{x}$ is one of the N particles, say $\boldsymbol{x}_j$ and $\boldsymbol{x}_{j_i}$ its neighbors of number $m(j)$, where $\boldsymbol{x}_j$ is distinct from $\boldsymbol{x}_{j_i}$, then we have the following sparse system of equations for the unknowns $\psi_j, j = 1, \ldots, N$

$$\psi_j - \sum_{i=1}^{m(j)} w_{j_i} \Bigg(Q_{11} + Q_{12} h_{1,j_i} + Q_{13} h_{2,j_i} + Q_{14} h_{3,j_i} + Q_{15} \frac{h^2_{1,j_i}}{2} +$$
$$Q_{16} h_{1,j_i} h_{2,j_i} + Q_{17} h_{1,j_i} h_{3,j_i} + Q_{18} \frac{h^2_{2,j_i}}{2} + Q_{19} h_{2,j_i} h_{3,j_i} + Q_{1,10} \frac{h^2_{3,i}}{2} \Bigg) \psi_{j_i} =$$
$$\left(Q_{11} A + Q_{12} B_1 + Q_{13} B_2 + Q_{14} B_3 + Q_{15} C + Q_{18} C + Q_{1,10} C \right) f +$$
$$\left(Q_{12} n_x + Q_{13} n_y + Q_{14} n_z \right) \phi.$$

and in matrix form

$$L\boldsymbol{\Psi} = \boldsymbol{R}. \qquad (42)$$

We have solved the above sparse system (42) using iterative methods like Gauss-Seidel and SOR. Since the values of the velocities and the pressure from time step n can be taken as initial values in the iterative methods for the time step $n + 1$, only very few iteration steps are required if the variation in time is not too large.

3.3 Numerical Tests

In the following we consider three examples in the two dimensional case. The test cases are given in dimensionless form but can be interpreted in SI-units.

Rayleigh-Taylor instability

In order to test our numerical scheme we first consider the Rayleigh-Taylor instability computed by the meshfree method SPH [4]. The authors have compared the SPH results with those from the VOF method. In this test case the heavy fluid lies above the light fluid. The computational domain is the rectangle $[0, 1] \times [0, 2]$. The densities of two fluids are 1.8 and 1. The dynamical viscosity of both fluids is $\mu = 0.4286 \times 10^{-3}$. The gravity acts downwards with $g = 1$. The Reynolds number is $Re = \rho UL/\mu = 420$ with $U = \sqrt{gL}$, $L = 1$.

Initially, we have considered 5147 particles with smoothing length $h = 0.6$. The initial interface is given by $1 - 0.15 \sin(2\pi x)$. The heavy particles (stars) lie on and above this interface and the rest are light ones (dots). No-slip boundary conditions are applied at the solid walls.

The time evolutions of the simulation are plotted in Fig. 2. Qualitatively, the results seem to be better than those obtained by the SPH method in [4].

Breaking dam problem

This is a classical and simple test case to validate numerical schemes for the simulation of free surface flows. In [19] experimental data are given and several authors have reported their numerical results [13, 18, 26, 27].

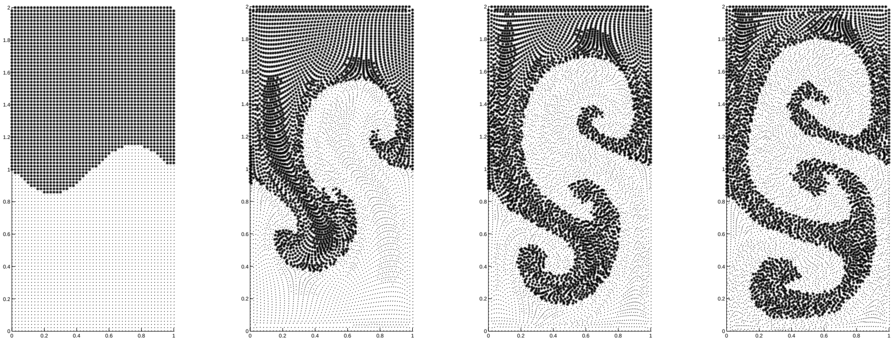

Fig. 2. Rayleigh-Taylor instability from left to right at time $t = 0, 3, 4, 5$

The computational domain is a rectangle with the size of $[0, 0.6] \times [0, 0.3]$. Consider a rectangular column of water with a width of $a = 0.1$ and a height of 0.2. The rest of the domain is filled with air. In Fig. 3 the star particles represent the water and the dot particles represent the air. No-slip boundary conditions are applied at all boundaries.

Initially, 5624 particles are distributed with smoothing length $h = 0.015$. The gravity with $g = 9.81$ acts downwards. The density of air is 1 and the viscosity is $1.81 \times 10.^{-5}$. For water the density is 1000 and the viscosity is 1.005×10^{-3}.

In Fig. 3 we have plotted the simulation results at different times. Since the density ratio of the fluids is very high, we have to smooth the density and viscosity three times near the interface in order to avoid numerical instabilities. If the density ratio is 100:1, it is enough to smooth the density at the interface only once. For the viscosity, also three smoothing steps are used, but the number of smoothing steps is less significant in this case.

In Fig. 4 the positions of the leading fluid front versus time as well as the heights of the water column versus time are compared with experimental results provided by [19]. The front position is computed as the maximum distance among the water particle from the origin. Similarly, the height is obtained from the maximum height of the water particles. The data are plotted before the particles hit the right wall. The numerical computations are performed with different values of h. The results are plotted for $h = 0.04, 0.02, 0.01, 0.005$ which correspond to the number of particles 400, 3117, 12593 and 49262 respectively. These figures show a good agreement between the numerical and experimental results for small values of h.

The CPU time in a PC Pentium 4, $2.66 GHz$ for different values of h are presented in table 1. In all cases the time step $\Delta t = 0.002$ has chosen and the program was terminated at time $t = 0.4$.

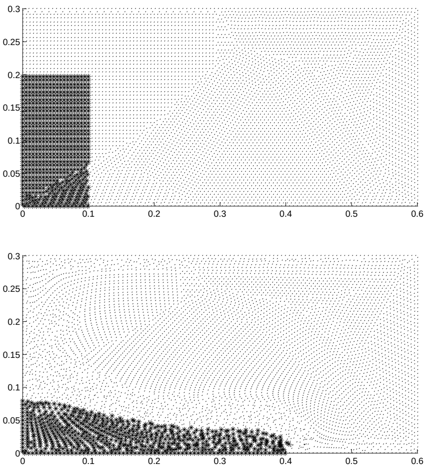

Fig. 3. star: water, dot: air particles at time $t = 0, 0.12, 0.24, 0.72$.

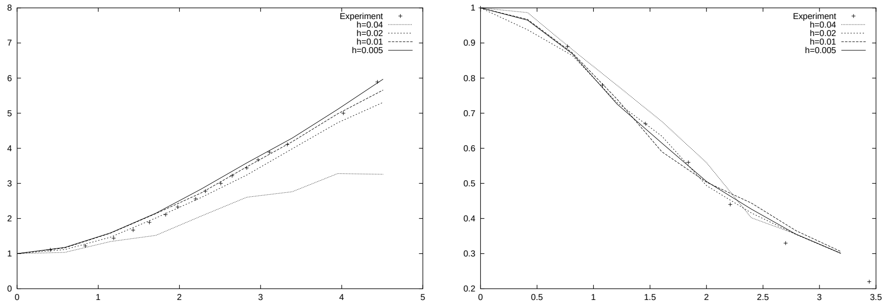

Fig. 4. Left: dimensionless front position x/a versus dimensionless time $t\sqrt{2g/a}$, right: dimensionless column height $x/(2a)$ versus dimensionless time $t\sqrt{g/a}$.

Table 1.

h	No of Particles	CPU time
0.04	800	0 Min 31 Sec
0.02	3117	2 Min 10 Sec
0.01	12593	9 Min 48 Sec
0.005	49262	46 Min 14 Sec

Droplet splash

Finally, we consider a water droplet falling through air onto a water surface. This problem was originally proposed in [20] and later reconsidered in [21] to test numerical schemes for variable density flows. The computational domain and the resolution is the same as in the test case of the Rayleigh-Taylor instability. The particles inside the circle of radius 0.2 with center $(0.5, 1.6)$ and below the line $y = 1$ are considered as water particles and the rest air particles. The other data are chosen as in the case of the breaking dam problem. These results are consistent with the results shown in [20, 21].

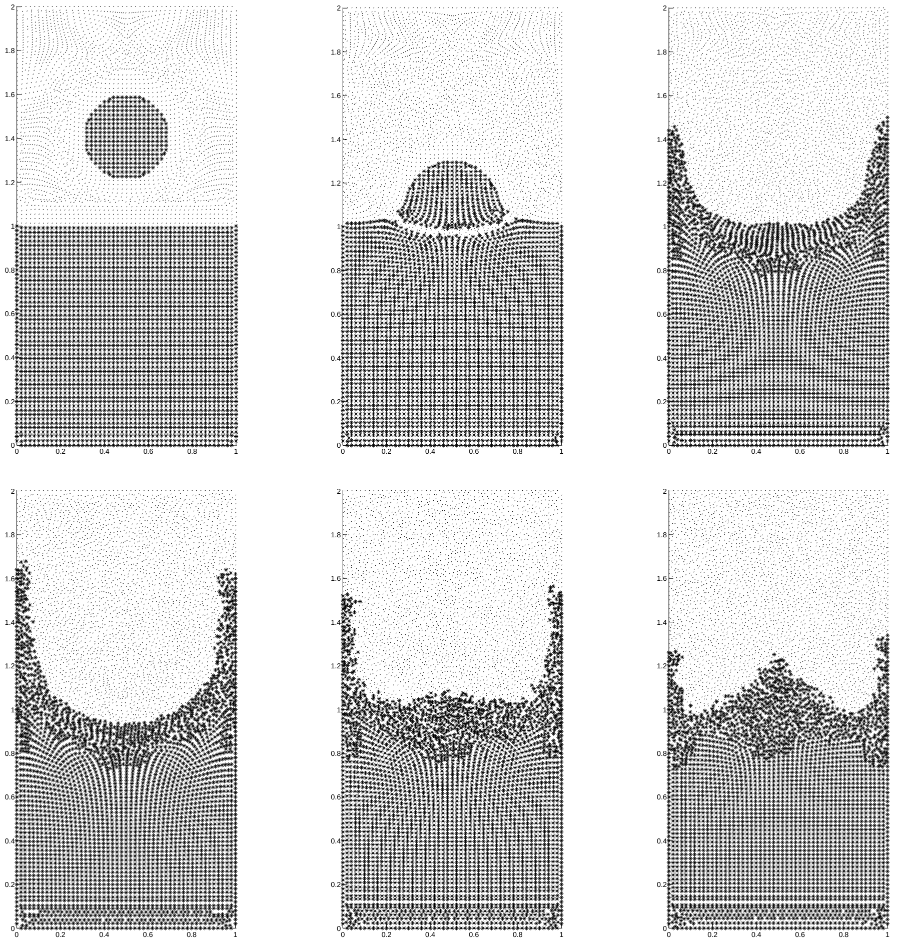

Fig. 5. Falling water droplet through air onto water surface from left to right and top to bottom at times $t = 0.2, 0.32, 0.48, 0.64, 0.88, 1.0$.

Acknowledgement

This work has been carried out in the project *Particle Methods for Conservation Systems* NE 269/11-3 which is part of the DFG – Priority Research Program *Analysis and Numerics for Conservation Laws.*

References

1. C. Chainais-Hillairet. Finite volume schemes for a nonlinear hyperbolic equation. Convergence towards the entropy solution and error estimate. M^2AN, 33:129–156, 1999.
2. A. Chorin. Numerical solution of the Navier-Stokes equations. *J. Math. Comput.*, 22:745–762, 1968.
3. B. Cockburn, F. Coquel, and P. LeFloch. An error estimate for finite volume methods for multidimensional conservation laws. *Math. Comput.*, 63:77–103, 1994.
4. S. J. Cummins and M. Rudmann. An SPH projection method. *J. Comput. Phys.*, 152:284–607, 1999.
5. G. A. Dilts. Moving least squared particle hydrodynamics – i. consistency and stability. *Int. J. Numer. Mech. Eng.*, 44:1115–1155, 1999.
6. E. Godlewski and P.-A. Raviart. *Numerical Approximation of Hyperbolic Systems of Conservation Laws.* Springer, 1996.
7. D. Hietel, K. Steiner, and J. Struckmeier. A finite-volume particle method for compressible flows. *Math. Models Methods Appl. Sci.*, 10:1363–1382, 2000.
8. J.M. Melenk I. Babushka, I. The partition of unity method. *International Journal of Numerical Methods in Engineering*, 40:727–758, 1997.
9. O. Iliev and Tiwari S. A generalized (meshfree) finite difference discretization for elliptic interface problems. In I. Dimov, I. Lirkov, S. Margenov, and Z. Zlatev, editors, *Numerical Methods and Applications*, Lecture notes in Computer Sciences. Springer, to appear.
10. Monaghan J. J. Smoothed particle hydrodynamics 1990. *Annu. Rev. Astron. Astrop*, 30:543–574, 1992.
11. M. Junk and J. Struckmeier. Consistency analysis for mesh-free methods for conservation laws. *Mitt. Ges. Angew. Math. Mech.*, 24:99–126, 2001.
12. R. Keck. *The finite volume particle method.* PhD thesis, Universität Kaiserslautern, 2003.
13. F. J. Kelecy and Pletcher R. H. The development of free surface capturing approach for multidimensional free surface flows in closed containers. *J. Comput. Phys.*, 138:939, 1997.
14. D. Kröner. *Numerical Schemes for Conservation Laws.* Wiley Teubner, 1997.
15. J. Kuhnert. *General smoothed particle hydrodynamics.* PhD thesis, Universität Kaiserslautern, 1999.
16. J. Kuhnert. An upwind finite pointset method for compressible Euler and Navier-Stokes equations. In M. Griebel and M. A. Schweitzer, editors, *Meshfree methods for Partial Differential Equations*, volume 26 of *Lecture Notes in Computational Science and Engineering.* Springer, 2002.

17. T. Liszka and J. Orkisz. The finite difference method on arbitrary irregular grid and its application in applied mechanics. *Computers & Structures*, 11:83–95, 1980.
18. V. Maronnier, Picasso. M., and J. Rappaz. Numerical simulation of free surface flows. *J. Comput. Phys.*, 155:439, 1999.
19. J. C. Martin and Moyce. M. J. An experimental study of the collapse of liquid columns on a liquid horizontal plate. *Phil. Trans. Roy. Soc. London Ser. A*, 244:312, 1952.
20. E. G. Puckett, A. S. Almgren, J. B. Bell, D. L. Marcus, and W. J. Rider. A high-order projection method for tracking fluid interfaces in variable density incompressible flows. *J. Comput. Phys.*, 130:269–282, 1997.
21. T. Schneider, N. Botta, K. J. Geratz, and R. Klein. Extension of finite volume compressible flow solvers to multi-dimensional. variable density zero Mach number flows. *J. Comput. Phys.*, 155:248–286, 1999.
22. D. Shepard. A two-dimensional interpolation function for irregularly spaced points. *Proceedings of A.C.M National Conference*, pages 517–524, 1968.
23. Y. Y. Lu T. Belytschko and L. Gu. Element-free Galerkin methods. *Int. J. Num. Methods in Engineering*, 37:229–256, 1994.
24. D. Teleaga. Numerical studies of a finite-volume particle method for conservation laws. Master's thesis, Universität Kaiserslautern, 2000.
25. S. Tiwari. A LSQ-SPH approach for compressible viscous flows. In H. Freistuehler and G. Warnecke, editors, *proceedings of HYP2000*, volume 141. Birkhäuser, 2001.
26. S. Tiwari and J. Kuhnert. Grid free method for solving Poisson equation. Technical report, Fraunhofer ITWM, Kaiserslautern, Germany, 2001.
27. S. Tiwari and J. Kuhnert. Finite pointset method based on the projection method for simulations of the incompressible Navier-Stokes equations. In M. Griebel and M. A. Schweitzer, editors, *Meshfree methods for Partial Differential Equations*, volume 26 of *Lecture Notes in Computational Science and Engineering*. Springer, 2002.
28. S. Tiwari and S. Manservisi. Modeling incompressible Navier-Stokes flows by lsq-sph. *Nepal Mathematical Sciences Report*, 20, 2003.
29. J.-P. Vila. Convergence and error estimates in finite volume schemes for general multidimensional scalar conservation laws. I. Explicit monotone schemes. M^2AN, 28:267–295, 1994.
30. Y.F. Zhang W.K. Liu, S. Jun. Reproducing kernel particle method. *Int. J. Num. Meth. in Fluids*, 20:1081–1106, 1995.
31. Z. Yang. Efficient calculation of geometric parameters in the finite volume particle method. Master's thesis, Universität Kaiserslautern, 2001.